LANGMUIR

pubs.acs.org/Langmuir Article

Interplay of the Assembly Conditions on Drug Transport Mechanisms in Polyelectrolyte Multilayer Films

Rogério A. Bataglioli,* João Batista M. Rocha Neto, Bruno S. Leão, Luiz Guilherme L. Germiniani, Thiago B. Taketa, and Marisa M. Beppu

Cite This: *Langmuir* 2020, 36, 12532−12544 Read Online

ACCESS | Metrics & More | Article Recommendations | Supporting Information

ABSTRACT: The layer-by-layer film deposition is a suitable strategy for the design and functionalization of drug carriers with superior performance, which still lacks information describing the influence of assembly conditions on the mechanisms governing the drug release process. Herein, traditional poly(acrylic acid)/poly(allylamine) polyelectrolyte multilayers (PEM) were explored as a platform to study the influence of the assembly conditions such as pH, drug loading method, and capping layer deposition on the mechanisms that control the release of calcein, the chosen model drug, from PEM. Films with 20−40 bilayers were assembled at pH 4.5 or 8.8, and the drug loading process was carried out during- or post-film assembly. Release data were fitted to three release models, namely, Higuchi, Ritger−Peppas, and Berens−Hopfenberg, to investigate the mechanism governing the drug transport, such as the apparent diffusion and the relaxation time. The postassembly drug loading method leads to a higher drug loading capacity than the during-assembly method, attributed to the washing out of calcein during film assembly steps in the latter method. Higuchi's and Ritger−Peppas' model analyses indicate that the release kinetic constant increased with the number of bilayers for the postassembly method. The opposite trend is observed for the during-assembly method. The Berens−Hopfenberg release model enabled the decoupling of each drug transport mechanism's contribution, indicating the increase of the diffusion contribution with the number of bilayers for the postassembly method at pH 4.5 and the increase of the polymer relaxation contribution for the during-assembly method at pH 8.8. Deborah's number, which represents the ratio of the polymer relaxation time to the diffusion time, follows the trends observed for the relaxation contribution for the conditions investigated. The deposition of the capping phospholipid layer over the payload also favored the polymer relaxation contribution in the drug release, featuring new strategies to investigate the drug release in PEM.

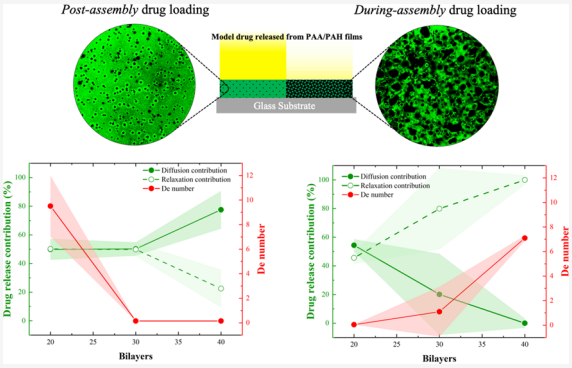

INTRODUCTION

Surface functionalization with nanostructured films has been explored to overcome biomedical challenges, designing antifouling surfaces,[1] coatings with antibacterial[2] and viral-killing[3] properties, and devices for the selective capture of active agents for diagnosing[4,5] and the delivery of therapeutics.[6] An analytical approach to methodically design and optimize polymer-based coatings for the efficient delivery of specific drugs is highly necessary because of the diversity of possibilities for physical and chemical interactions between drugs and selected polymeric materials,[7−9] in addition to the interaction of biomaterial accordingly to the environmental stimuli.[10] Amongst the methods used for the film assembly,[11,12] the layer-by-layer (LbL) technique has emerged as one of the most popular strategies for the self-assembly of polyelectrolyte multilayers (PEM) through the interaction of oppositely charged species,[13] enabling one to tune the surface properties based on the assembly conditions,[14] the sequence of building block deposition,[15] or the postassembly treatment.[16]

Several features make the LbL films attractive for drug delivery, including the control of the drug loading and release processes, the ability to functionalize surfaces with diverse geometry and chemistry, the use of mild chemical conditions for handling sensitive therapeutic molecules, and the simple and scalable processing.[17] These features have led to the design and investigation of a multilayer core−shell structure for the encapsulation and sustained release of dyes,[18] small drugs,[19,20] enzymes,[21] proteins,[22,23] and DNA molecules.[24] LbL films have also been deposited over drug particles,[25,26] nanogels,[27,28] liposomes,[29,30] nanotubes,[31] and magnetic nanoparticles,[32] aiming to increase the stability and avoid undesired burst release effects. Alternative methods for drug loading on

Received: July 6, 2020
Revised: October 3, 2020
Published: October 16, 2020

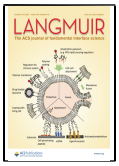

https://dx.doi.org/10.1021/acs.langmuir.0c01980
Langmuir 2020, 36, 12532−12544

multilayer film structures have also been reported. For example, Wood and co-workers designed hydrolytically degradable films of poly(β-amino ester) and therapeutic polysaccharides for drug release applications based on film erosion.[33] This concept has been explored as a strategy to control the release rate of film constituents based on film architecture and composition,[17] and more recently, to create a temporal-controlled release of multiprotein formulations for vaccine applications.[23] Rubner and co-workers have explored postassembly drug loading methods in weak-polyelectrolyte-based films,[34,35] such as the adsorption of charged dye molecules via electrostatic interaction with unbound oppositely charged groups[34] and the entrapment of small organic drug molecules into porous structures via capillary condensation.[35] These methods present a strong dependence of the pH for controlling the number of charged groups in the PEM[34] or forming a porous structure after the film assembly,[36] illustrating the importance of the assembly conditions on the drug delivery properties of PEM.

Mathematical models are valuable tools to investigate the performance of drug delivery devices,[37] clarifying the role of the structure in their final performance. The underlying assumptions of these models reflect the mechanisms governing drug transport in each system. For example, the traditional Higuchi model describes the release of water-soluble drugs from solid or semisolid matrices,[38] while the first-order release model represents a concentration-dependent drug release process. Semiempirical models, such as the Ritger−Peppas model or the power-law model, help us to elucidate the predominance of diffusion- or relaxation-controlled mechanisms, or the superposition of both (anomalous release), in the drug release process,[39] while the Berens−Hopfenberg model enables one to decouple the contribution of each mechanism.[40] Several studies have reported the use of release models as tools for investigating the drug delivery performance of LbL films. Anirudhan and co-workers described the controlled release of 5-fluorouracil for cancer treatment from aminated mesoporous silica nanoparticles coated with hyaluronic acid/chitosan multilayers.[20] The authors observed the best fit for the power-law model with the predominance of the anomalous release. Other studies also observed the same behavior for devices with different geometries such as nanotubes,[31] capsules,[19] liposomes,[29,30] and thin films,[41] lacking a description of the individual contribution of the diffusion and relaxation mechanisms for the overall release process. Tan and co-workers investigated the release of procaine hydrochloride from methacrylic acid-ethyl acrylate gel particles coated with poly(allylamine hydrochloride)/poly(sodium 4-styrene sulfonate) using the Berens−Hopfenberg model.[27] The authors described both the increase of the relaxation time and the decrease in the diffusion coefficient with the number of bilayers deposited, suggesting that the film assembly conditions may play a role in the contribution of each mechanism for the drug release process.

This study aims to investigate the influence of the film assembly conditions on the specific mechanisms controlling the drug release process. The polymeric drug delivery system was engineered in such a way that the loading and kinetic release of the selected model drug could be adjusted by experimental parameters that directly influence the configuration of polymeric structures, such as pH, ionic strength, and postassembly treatments, with the latter including calcein incorporation and deposition of a capping film. Poly(acrylic acid)/poly(allylamine hydrochloride) multilayer films were assembled over glass substrates using the dipping LbL method at pH 4.5 or 8.8. Calcein, the model drug chosen here, was loaded into the PEM during- or post-film assembly, followed by the addition of a capping film on top of the payload. The surface and bulk film morphology were probed using the traditional profilometry, atomic force microscopy (AFM), and confocal microscopy techniques, while chemical changes in the PEM were investigated by UV−visible spectroscopy and coupled AFM-IR techniques. Polyelectrolyte solution properties were assessed using ζ-potential and dynamic light scattering (DLS) analyses to understand the interplay of assembly parameters and film structures. Drug release data were fitted to three different release models to understand the influence of assembly parameters on the mechanisms that govern the drug transport in PEM. Understanding the interplay between the structure and release properties may give incremental insights into the design of the next generation of drug delivery devices.

MATERIALS AND METHODS

Materials. Poly(acrylic acid) (PAA, ∼100 kDa, 35% w/w aqueous solution), poly(allylamine hydrochloride) (PAH, ∼15 kDa), polyethyleneimine (PEI, ∼750 kDa, 50% w/w aqueous solution), calcein (CAL), L-α-phosphatidylcholine (1,2-diacyl-sn-glycero-3-phosphocholine, from egg yolk), and phosphate-buffered saline (PBS, pH 7.4 ± 0.1) were purchased from Sigma-Aldrich. These and other reagents were all of analytical degree and were used without further purification. Aqueous solutions were prepared with ultrapure water (18.2 MΩ·cm at 25 °C) from a Milli-Q ultrapure water system.

Methods. *Multilayered Film Assembly.* Polyelectrolyte multilayers were assembled over microscopic glass slides (Kasvi, 15 × 15 × 1.2 mm^3) using a programmable homemade dipping machine. Before PEM deposition, glass slides were sequentially cleaned in an ultrasound bath (Cristofoli, Brazil) with a 1% v/v commercial detergent solution, 1.0 M sodium hydroxide solution, and ultrapure water for 16 min each, and dried with blow air.[42] The glass slides were then immersed into a PEI solution (1 g/L, 100 mM NaCl, at pH 4.0) for 15 min, followed by three rinse steps (pH 4.0) with ultrapure water for 1 min each, as described elsewhere.[42] (PAAx/PAHx)n films with the number of bilayers, n, ranging from 20 to 40 bilayers were assembled from solutions PAA and PAH solutions (10 mM, based on the repeat unit molecular weight, and 50 mM NaCl) both at pH, x, 4.5 or 8.8. PEM were deposited over the glass substrates by immersion cycles into the polyelectrolyte solutions for 15 min each, alternated by three rinse steps for 1 min each in ultrapure water at the same pH. After film deposition, the samples were stored in a vacuum desiccator for at least 24 h before use. The samples were prepared in triplicate for each condition tested.

Solution ζ-Potential and DLS Measurements. Dynamic light scattering (DLS) and ζ-potential measurements of polyelectrolyte solutions were carried out using a universal dip cell and polystyrene cuvettes in Malvern Zetasizer Nano ZS equipment. All samples were prepared in triplicate at 1.0 mg/mL and syringe filtered through a Chromafil PES 0.2 μm filter right before the measurements. Data were treated using Zetasizer software (Malvern, England).

Drug Loading. CAL was loaded into the PEM using two different methods: during- and post-film deposition. In the traditional method, PEM were immersed into the CAL solution (60 mg/L, pH 7.1) for 24 h, followed by three rinse steps for 1 min each and one drying step at room temperature. In the alternative method, CAL was loaded during each PEM deposition cycle; after one single PAA/PAH deposition, wet PEM were immersed into CAL solution (pH 7.1) for 15 min, followed by three rinse steps at the same pH for 1 min each, and the cycle was repeated for the number of bilayers desired. For both methods, all sample handling steps were conducted protected from light exposure. All samples had their absorbance spectra recorded at a range of 400−650 nm wavelength.

Spin-Coated Capping Film Deposition. PAA/PAH films with 40 bilayers loaded with CAL (payload) were coated with a capping film through the spin coater method (Model WS-650-MZ, Laurell). PAA/PAH films were deposited over the payload region by adding 150 μL of

https://dx.doi.org/10.1021/acs.langmuir.0c01980
Langmuir 2020, 36, 12532−12544

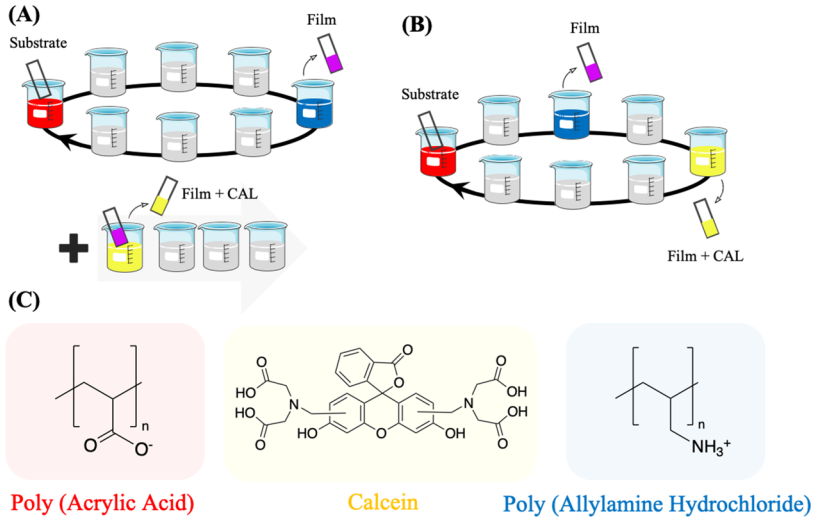

Figure 1. Schematic representation of multilayer film assembly and drug loading methods. Polyelectrolyte multilayer films were assembled using the layer-by-layer method with CAL, the model drug molecule, loaded into the films (A) post- or (B) during-assembly through the dipping method. (C) Representation of the polyelectrolytes' chemical structure forming the film and the model drug molecule loaded into the films.

each polyelectrolyte's solution (1 g/L at pH 4.5 or 8.8 for PAA/PAH) on the payload surface (15 × 15 mm^2), followed by spinning at 3000 rpm for 30 s. Bilayers were alternated deposited by washing steps with ultrapure water at the same pH and spinning conditions. Alternatively, a single layer of L-α-phosphatidylcholine was cast over the payload region by adding 150 μL of 2.0% w/v phospholipid solution in isopropanol, followed by spinning at 3000 rpm for 3 min.[43] All samples had their absorbance spectra recorded at a range of 400−650 nm wavelength before and after barrier deposition for detecting CAL loss and were used for drug release tests right after 12 h of barrier deposition.

Drug Release and Data Fitting. Release experiments were performed in 6-well plates containing 12 mL of PBS buffer, with the film vertically positioned over the well wall. The well plate was kept inside the plate reader (Varioskan Lux, Thermo Scientific), protected from light exposure, at 25 °C for, at least, 24 h. Fluorescence measurements with excitation and emission wavelengths of 490 and 540 nm, respectively, were performed right after 5 s shaking at 60 rpm. The residual amount of CAL in the PEM before and after the drug release was determined using the plate reader, in the absorbance mode, with dried PEM placed in the center of 6-well plates face side up. Peaks for CAL were observed at 480 and 505 nm. CAL release data were fitted to three different drug release models using the Levenberg−Marquardt algorithm for least-squares regression using Origin software. For the Higuchi and Ritger−Peppas models, data fitting was carried out using the first 60% of the total drug released,[39] while for the Berens−Hopfenberg model, the entire dataset was employed in the data fitting.[27] For both methods, the coefficient of determination and residual distribution were used to analyze the fitting models statistically.

Film Thickness. Film thickness was determined using a Dektak 150 profilometer (Veeco) by measuring the average height difference over a scratched line prepared over the film using a razor blade.[44] The scored line was scanned with a stylus set to apply a force of 100 mg over the surface at a scan speed of 17 μm/s. Thickness values are the average of five measurements performed in dried films at room temperature.

Film Surface Chemistry. Chemical changes after CAL loading were probed using an atomic force microscopy infrared spectroscopy technique. Measurements were performed on a NanoIR2 microscope (Anasys Instruments), using a silicon overall gold coating tip ContGB-G (BudgetSensors, Bulgaria) with <25 nm tip apex diameter, a nominal force constant of 0.2 N/m, and a nominal resonance frequency of 13 kHz at room temperature, and a relative humidity of approximately 5%. PAA/PAH films with 30 bilayers, with and without CAL loaded, were prepared over gold-coated silicon slides, and the IR spectra were collected within the range of 1550−1820 cm^{-1}, with a spectral resolution of 2 cm^{-1} per point in quintuplicates.[5] Image processing was carried out using open-source Gwyddion software.

Film Morphology Analyses. Film surface imaging was conducted using an atomic force microscope (AFM, Nanosurf Easyscan 2, Switzerland) under both controlled temperature and relative humidity (25 °C and 15−20% of RH). Dry films were assessed at a tapping mode by scanning square regions of 5 × 5 μm^2 size with 512 pts/line resolution using a silicon cantilever of a nominal constant spring of 40 N/m. Image processing and root-mean-square (RMS) roughness calculations were carried out in triplicate using open-source Gwyddion software. Film bulk morphology was assessed by images obtained using a confocal laser scanning microscope. Confocal images were obtained using an inverted confocal microscope Leica (TCS SP5 II, Leica, Germany). An excitation wavelength of 488 nm was used to image CAL in the film bulk with 100× objective. Confocal images were treated using ZEISS ZEN microscope software.

RESULTS AND DISCUSSION

Influence of PEM Assembly Conditions on Drug Loading. PAA/PAH films were chosen to investigate the role of the PEM structure in drug loading and release mechanisms because of the simplicity of their polymer chains and the pH-controlled ionization degree of both polyelectrolytes.[34] Several studies have explored the effects of charge density on PAA/PAH multilayer growth for a wide range of applications, including drug delivery,[34] antibacterial surfaces,[45] and antireflection coatings.[46] An in-depth understanding of film formation dynamics based on colloids' properties in solution has also been evaluated.[47,48] Inspired by these previous investigations, this study aims to understand the interplay of the colloids' properties in solution and surface modification's effect on the drug load and release properties, supported by mathematical models that help establish parameters related to the mass transfer mechanism that governs the release process. CAL was chosen as the model drug molecule for this study due to the simplicity in probing both its distribution into multilayered films and its drug release profile.[49]

The assembly pH promotes significant changes in polyelectrolyte chemical properties either in solution or in the PEM. PAA/PAH films were assembled at pH 4.5 or 8.8, corresponding to the values within the range where the pK_a of the PAA[36] and PAH[34] are included, respectively. At pH 4.5, carboxylate chains

https://dx.doi.org/10.1021/acs.langmuir.0c01980
Langmuir 2020, 36, 12532−12544

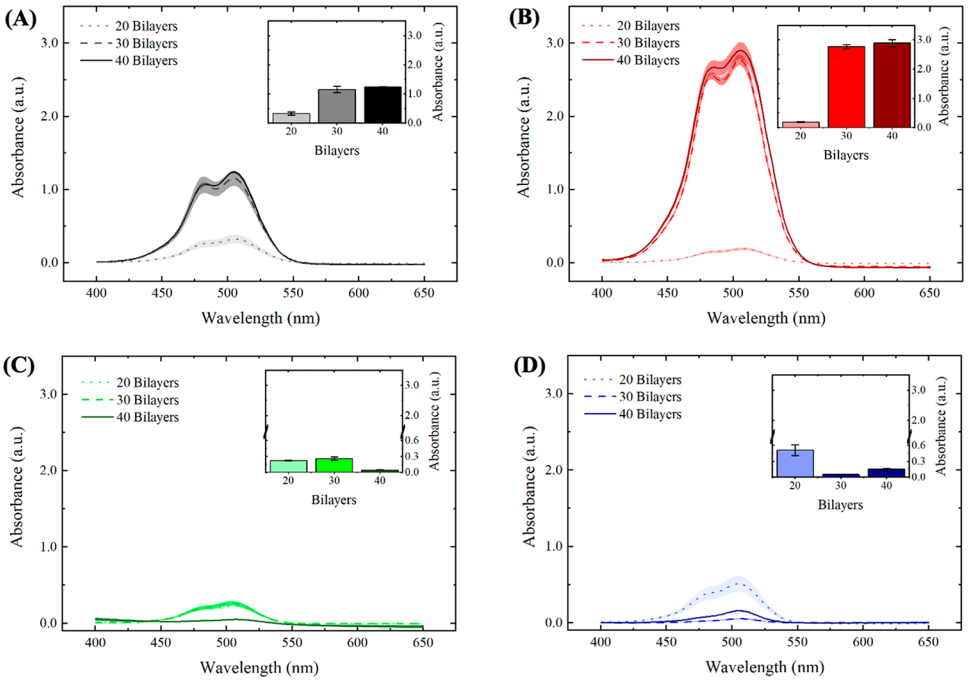

Figure 2. Absorbance spectra for PAA/PAH films after drug loading show an increase in the amount of CAL loaded for the postassembly drug loading method and a pH-dependent drug loading behavior for the during-assembly drug loading method. UV−visible spectra for PAA/PAH films assembled at (A) pH 4.5 and (B) pH 8.8 with CAL loaded after film assembly, and at (C) pH 4.5 and (D) pH 8.8 with CAL loaded during film assembly. Insets represent the absorbance peak at 505 nm. Shaded areas and error bars represent the standard error values.

from PAA are partially ionized, and amino groups from PAH are nearly fully ionized, while the opposite trend is observed at pH 8.8 (see ζ-potential results in Figure S1A). Modifications on PEM chemical composition due to changes in the assembled pH are observed in AFM-IR analysis, indicated by changes in the IR spectra peak at ∼1650 cm^{-1}. This band is assigned to the stretching of C═O of carboxylate groups, illustrating the influence of the film assembly pH in the PEM composition, particularly in the number of carboxylate groups in the PEM structure (Figure S2A−C).[5]

The drug model was loaded into the PEM using two different methods: the postassembly method and the during-assembly method, in which the drug was loaded during the deposition of the PEM (Figure 1). The increase in the IR spectra peaks at around 1600 and 1650 cm^{-1} correspond, respectively, to C═C stretches in aromatics and C═O stretches in the carboxylates[50] after the loading process validates the successful load of CAL into the PEM (Figure S2B−D). The amount of CAL loaded into the PEM was probed by UV−visible spectral analysis (Figure 2), which indicates the presence of a predominant peak at 505 nm for all conditions tested, reinforcing the successful load of CAL on the PEM structure. These spectra also presented a shoulder at 480 nm, particularly for films assembled with 30 and 40 bilayers. Wallach and co-workers reported the appearance of two bands for CAL in the 440−520 nm range attributed to different activation and absorption at acid, neutral, and alkaline medium.[51] The authors suggest that the acidic pH displaces the activation maxima from 445 to 460 and 475 nm, while the alkaline pH promotes the displacement to 475 and 500 nm with a slight decrease in the former.[51] Absorbance measurements for calcein solution (Figure S3C) corroborate to this trend, indicating a more prominent peak at 480 nm for the CAL solution at pH 4.5, which is also more pronounced in the spectra of PAA/PAH films assembled at the same pH conditions (Figure 2A−C). These results suggest that although the same neutral pH conditions of the calcein solution were employed for both loading methods, the assembly pH influences on both the CAL structure and the absorbance spectra. The appearance of the prominent shoulder near 475 nm for films containing 30 and 40 bilayers, regardless of the assembly conditions tested, may also be attributed to the decrease in the assembly pH of the polyelectrolyte solution throughout the film deposition.

Both assembly pH conditions resulted in higher loading capacities for the postassembly drug loading method (Figure 2A,B) compared to the during-assembly drug loading method (Figure 2C,D). This result is attributed to the longer contact time of the payload with the polyelectrolyte solutions and the rinsing water, which promotes a substantial drug leaking from the films prepared using the latter method, particularly in the PAA solution. The postassembly method has a minimal contact time with solution after drug loading (only the 1-min rinsing steps to remove unbound drug molecules, as described in the Experimental Methods). The postassembly drug loading process presented an increase in the absorbance peak at 505 nm, increasing the number of bilayers deposited from 20 to 30 (Figure 2A,B). Notably, both pH conditions investigated did not promote an increase in drug loaded into the films from 30 to 40 bilayers. This result may be explained by the film growth regimen observed for the PEM and the distribution of free ionized groups over the film structure near the outer film interface, as suggested by the three-zone model.[52] Multilayer film composed of two simple polyelectrolytes can be divided into three zones. Zone I is composed of one or a few layers of polyelectrolytes, close to the substrate, and the interfacial interaction of the polyelectrolytes with the substrate is strong. Zone II is the continuous medium (bulk) of the film, far from the possible influence of interfaces. The outermost zone, called Zone III, consists of a few layers of polyelectrolytes close to the

https://dx.doi.org/10.1021/acs.langmuir.0c01980
Langmuir 2020, 36, 12532−12544

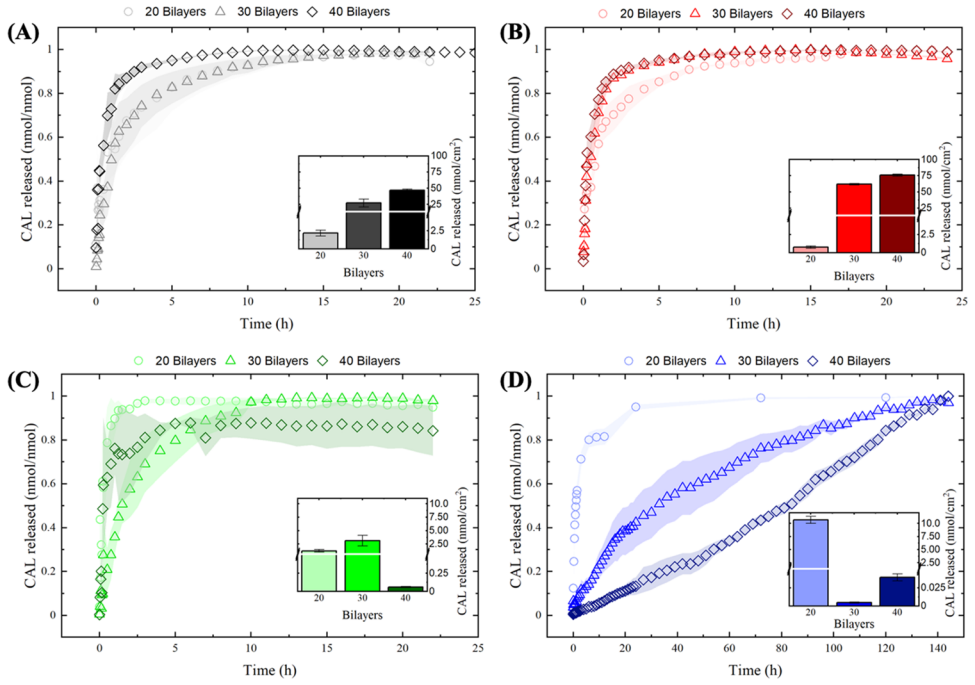

Figure 3. CAL release profiles show faster release kinetic profiles with an increase in the number of bilayers for the postassembly drug loading method. The opposite trend is observed for the during-assembly drug loading method. Drug release kinetic profiles for PAA/PAH films assembled at (A) pH 4.5 and (B) pH 8.8 with postassembly drug loading, and at (C) pH 4.5 and (D) pH 8.8 for during-assembly drug loading. Insets represent the total amount of CAL released. Shaded areas and error bars represent the standard error values.

film's outermost interface. In this zone, multilayers are influenced by the surface in contact with air or the hydration medium's solution.[52] According to the 3-zone model, by increasing the number of bilayers, the film thickness also increases; however, the number of free amino groups in the film, which are likely the sites where CAL interactions possibly occur, does not monotonically increase with the number of bilayers. This model suggests that the film has the largest number of free groups close to the interface with the aqueous solution, while the polyelectrolytes that make up the bulk (zone II) are complexed with each other, and then prevalently unavailable to interact with CAL.

The postassembly drug loading method also indicated higher absorbance values for films assembled at pH 8.8 (Figure 2B), compared to films assembled at pH 4.5 (Figure 2A). Taking into consideration the structure of both polymers and the polyanionic character of the CAL molecules, bearing four carboxylate groups ionized in the loading conditions, the uptake of CAL into the PEM is essentially mediated by the electrostatic interaction of carboxylate groups of CAL and free amino groups of PAH macromolecules until reaching the equilibrium between the bulk and the CAL solution (see Figure S3). Yoo and co-workers reported that assembly pH conditions that favor the partial ionization of carboxylate groups of PAA promoted superior cationic dye loading capacities into PAA/PAH films,[44] reinforcing that films assembled with partially ionized polyelectrolytes will present a higher amount of free, non-complexed, ionizable groups available for drug loading. The pH-dependence of the amount of free ionizable groups for weak polyelectrolyte multilayers agrees with the higher loading capacities observed for films assembled at pH 8.8 as a possible consequence of the highest amount of free amino groups in PAH chains.

To understand the drug loading method during film assembly, one must consider the release of CAL molecules over the entire assembly process, which is associated with (1) the CAL chemical potential difference between the film bulk and both polyelectrolyte solutions and rinse water, and (2) the ionic exchange between the adsorbed CAL molecules into the PEM and the newly adsorbed PAA chains.[14] These factors reduce the CAL peak intensity in the films, making the drug loading process into the PEM dependent on the net material balance. Films loaded with CAL during the assembly process showed a behavior dependent on both the pH and the number of bilayers (Figure 2C,D). At pH 4.5, the CAL-loaded films presented a maximum at 30 bilayers (Figure 2C, inset), while at pH 8.8, the CAL loading process resulted in a minimum at 30 bilayers (Figure 2D, inset). These opposite trends indicate that the interplay between the drug uptake and release during assembly, which controls the CAL-loading capacity, presents a pH-dependent behavior. The maximum peak intensity observed at pH 4.5 suggests that the total amount of drug loaded is mediated by a competition between the drug uptake and the drug release during the assembly process, which is disfavored by the increase in the number of bilayers deposited. At pH 8.8, the higher ionization degree of PAA may have a more substantial impact on the drug removal from the PEM during the loading process. For the initial layers deposited at pH 8.8, fully charged PAA molecules tend to displace a more substantial amount of CAL compared to films assembled at pH 4.5, surpassing the rate of drug uptake in the films. As the number of layers deposited increases, the amount of CAL released into the PAA solution reduces the chemical potential between the film and the polyanion solution, also reducing the amount of CAL released during the assembly process, thereby favoring the increase in the absorbance peak observed for films with 40 bilayers. The use of the during-assembly drug loading method aimed to promote a homoge-

https://dx.doi.org/10.1021/acs.langmuir.0c01980
Langmuir 2020, 36, 12532−12544

Table 1. Release Kinetic Models and Their Corresponding Mathematical Equations[a]

release kinetic model	mathematical equation	remarks
Higuchi[38]	$\frac{M_t}{M_\infty} = k_H t^{1/2}$	M_t—amount of drug released at time t
		M_∞—total amount of drug released along the process
Ritger–Peppas[39]	$\frac{M_t}{M_\infty} = k_P t^n$	k_H—Higuchi kinetic constant
		k_P—Ritger-Peppas kinetic constant
		n—release exponent
Berens–Hopfenberg[40]	$\frac{M_t}{M_\infty} = 1 - \varnothing_F\left[\frac{6}{\pi^2}\sum_{n=1}^{\infty}\frac{1}{n^2}e^{-n^2 k_F t}\right] - \varnothing_R e^{-k_R t}$	$\varnothing_F$—fractional diffusion contribution
		$\varnothing_R$—fractional chain relaxation contribution
	$k_R = 1/\tau$	k_F—diffusion constant
		k_R— first-order chain relaxation constant
	$k_F = \frac{4\pi^2 D}{d^2}$	D—diffusion coefficient
		d—film thickness
		τ—characteristic chain relaxation time

[a]The value of the release exponent in the Ritger–Peppas model provides information regarding the drug release mechanism: $n = 0.5$—Fickian, or diffusion-controlled release; $0.5 < n < 1.0$—anomalous, or both diffusion- and polymer relaxation-controlled mechanism; $n = 1.0$—non-Fickian, or relaxation-controlled release.[39]

neous distribution of CAL over the film structure, creating a more sustained release profile. However, the substantial reduction in the amount of drug loaded compared to the traditional method highlights the importance of reducing the contact time between the payload and aqueous medium to minimize drug leaking.

PEM Release Kinetic Profile and Modeling. To address the role of the film assembly conditions in the drug release profile, CAL release data were normalized to the total amount of drug released in each condition tested (Figure 3). Most of the assembly conditions tested were able to release most of the drug in the first 24 h of the experiment (film absorbance spectra after CAL release are presented in Figure S4). Films assembled at pH 8.8 with drug loading during film deposition, however, showed slower release kinetic profiles and took 6 days to release most of the CAL adsorbed.

Different drug release patterns were observed depending on the drug loading method employed. Films prepared using the postassembly drug loading method presented faster drug release kinetic profiles as the number of bilayers increases, regardless of the pH conditions. This qualitative assessment was carried out by looking at the fractional amount of drug released at a time to all conditions studied. This trend may be associated with the burst release effect that is typically proportional to the total amount of drug loaded into the films represented in the insets in Figure 3. Conversely, films loaded with CAL during the assembly process presented a reduction in the release kinetic profiles with the number of bilayers deposited, particularly for films assembled at pH 8.8. Here, the burst release seems to be less significant as the number of bilayers deposited increases, and other factors may influence the release kinetic profiles, attributed to the stronger binding between the drug and the polymer matrix due to the removal of moderate to weakly bound CAL molecules during the sequential assembly steps.

Mathematical models have been commonly employed for the quantitative analysis of drug release systems, enabling the assessment of the mechanisms that drive the release process. Release kinetic data were fitted to three different models (Table 1), each of them providing relevant information regarding the drug release mechanism in the PAA/PAH films (Table 2). The cumulative amount of CAL released for each film was calculated from fluorescence measurements and normalized by the film surface area and the total amount of drug release in each case, to determine the amount of CAL released over time.

Higuchi's model was the first equation developed to represent a drug release process. This model assumes that the transport of molecules out of the polymeric matrix is the only mechanism governing the release process.[38] Recently, Wang and co-workers reported the application of the Higuchi model to fit the *in vitro* dual release of cancer drug molecules from chitosan/dextran sulfate LbL-coated nanoparticles.[53] Zhao and co-workers employed the same model to determine the apparent diffusion constant of the antitumor drug doxorubicin from chitosan/alginate multilayer microcapsules, obtaining constants over the range of 8.8×10^{-8}–5.4×10^{-7} cm^2/s.[54] The analysis of the kinetic constants (Table 2) for the Higuchi model, k_H, corroborates the release profiles observed in Figure 3, showing higher values for the postassembly drug loading method compared to the during-assembly method at the same pH for nearly all cases studied. The increase in the kinetic constant with the number of bilayers deposited was also observed at pH 8.8 for the former method, while the latter one shows a decrease in the kinetic constant at the same pH. Of note, the limited quality of the data fit observed for this model, illustrated by the correlation coefficient value ($\leq$0.9), suggests that the release process is not entirely diffusional, limiting any further analysis of the retrieved parameters.

CAL release data were also fitted to the Ritger–Peppas or power-law model, a semiempirical model to describe the drug release from polymeric systems.[39] This model characterizes the drug transport as diffusion-controlled, polymer relaxation-controlled, or a combination of both mechanisms, according to the value of the release exponent, n. The release kinetic constant, k_P, values obtained show the same trends observed for the Higuchi model (Table 2). From the values of the exponent of release, n, most assembly conditions investigated presented an anomalous release, indicating that both diffusional and relaxation mechanisms contribute to the drug transport. The only exceptions are the films with 20 bilayers, which presented a diffusion-controlled release ($n < 0.5$). The anomalous release profile for PEM is also observed in a previous paper for the release of the rose bengal dye from LbL films of carbox-

https://dx.doi.org/10.1021/acs.langmuir.0c01980
Langmuir 2020, 36, 12532–12544

Table 2. Release Kinetic Model Parameters for PAA/PAH Films Assembled at pH 4.5 and pH 8.8 with Post- or During-Assembly Drug Loading Methods[a]

film assembly conditions		Higuchi		Ritger–Peppas			Berens–Hopfenberg							
		k_H	R^2	k_p	n	R^2	θ_F	k_F	θ_R	k_R	$D/10^{-15}$ (cm^2/s)	$\tau/10^4$ (s)	De	R^2
pH 4.5—CAL after	20	0.550 (0.036)	0.753	0.529 (0.033)	0.347 (0.063)	0.814	0.498 (0.073)	1.952 (0.809)	0.501 (0.073)	0.205 (0.035)	28.824 (6.938)	1.753 (0.175)	9.507 (2.466)	0.972
	30	0.468 (0.019)	0.949	0.482 (0.009)	0.681 (0.033)	0.988	0.501 (0.046)	0.139 (0.013)	0.498 (0.046)	0.927 (0.054)	5.324 (0.349)	0.388 (0.013)	0.150 (0.009)	0.997
	40	0.840 (0.049)	0.862	0.778 (0.080)	0.426 (0.077)	0.859	0.774 (0.131)	0.649 (0.120)	0.225 (0.131)	4.200 (1.178)	75.23 (8.61)	0.085 (0.013)	0.154 (0.030)	0.982
pH 8.8—CAL after	20	0.590 (0.028)	0.894	0.563 (0.028)	0.399 (0.049)	0.917	0.811 (0.043)	0.244 (0.022)	0.188 (0.043)	6.310 (1.925)	9.612 (0.627)	0.057 (0.01)	0.038 (0.007)	0.988
	30	0.746 (0.046)	0.883	0.755 (0.083)	0.512 (0.090)	0.867	0.541 (0.091)	0.381 (0.076)	0.458 (0.091)	2.707 (0.329)	92.74 (11.86)	0.132 (0.009)	0.140 (0.019)	0.987
	40	0.907 (0.053)	0.910	0.980 (0.142)	0.555 (0.097)	0.902	0.903 (0.061)	1.241 (0.215)	0.096 (0.061)	0.167 (0.103)	915.4 (93.22)	2.144 (0.767)	7.396 (2.746)	0.988
pH 4.5—CAL during	20	1.032 (0.188)	0.446	0.631 (0.521)	0.253 (0.387)	0.344	0.650 (0.324)	1.587 (1.026)	0.349 (0.324)	3.019 (2.964)	11.55 (4.32)	0.119 (0.067)	0.525 (0.357)	0.931
	30	0.380 (0.017)	0.932	0.367 (0.016)	0.630 (0.059)	0.950	0.450 (0.078)	0.190 (0.036)	0.549 (0.078)	0.415 (0.053)	5.356 (0.599)	0.866 (0.064)	0.459 (0.060)	0.993
	40	0.831 (0.112)	0.715	1.170 (0.349)	0.753 (0.223)	0.739	0.849 (0.040)	1.162 (0.233)	0.150 (0.040)	0.005 (0.019)	86.57 (10.08)	66.90 (143.2)	216.1 (463.3)	0.925
pH 8.8—CAL during	20	0.463 (0.011)	0.949	0.475 (0.008)	0.415 (0.025)	0.976	0.543 (0.042)	0.071 (0.010)	0.456 (0.042)	1.529 (0.150)	12.86 (1.37)	0.235 (0.013)	0.046 (0.004)	0.995
	30	0.086 (0.000)	0.978	0.057 (0.002)	0.619 (0.013)	0.992	0.200 (0.283)	0.021 (0.067)	0.799 (0.283)	0.019 (0.006)	17.08 (31.38)	18.71 (3.75)	1.098 (2.034)	0.995
	40	0.046 (0.001)	0.836	0.003 (0.000)	1.134 (0.008)	0.998	0.000 (0.032)	0.074 (0.000)	1.000 (0.032)	0.010 (0.000)	104.8 (5.3)	34.06 (1.00)	7.094 (0.209)	0.899

[a]Standard error values are presented in parenthesis.

ymethylcellulose/chitosan,[41] with a lack of further information regarding the quantitative contribution of the diffusional and the polymer relaxation mechanisms for the drug release process.

The Berens–Hopfenberg model enabled the assessment of the individual contribution of each mechanism for CAL release in PEM (Table 2). This model takes into consideration the effect of the polymer swelling and the chain relaxation into the drug diffusion through the polymer matrix, making the drug transport dependent on both the polymer chain relaxation rate and the drug diffusion rate.[40] The parameters retrieved from this model show an increase in the diffusional contribution with the number of bilayers for the postassembly drug loading at pH 4.5, with the opposite trend observed during-assembly drug loading at pH 8.8. The kinetic parameters for both transport mechanisms also enable the calculation of the apparent diffusion coefficient, D, of the drug in the film and the relaxation time, τ, of the polymer chains (see equations for k_F and k_R in Table 1). The diffusion coefficients increase with the number of bilayers for nearly all cases studied, except for films with 30 bilayers at pH 4.5 for both drug loading methods. Polymer relaxation time values indicate an increase with the number of bilayers deposited for the during-assembly drug loading method, at both pH values, and for the postassembly drug loading at pH 8.8. The only exception was the films assembled at pH 4.5, with postassembly drug loading, which showed a reduction in the relaxation time with the number of bilayers deposited. Tan and co-workers reported the values of D and τ for the drug release from 200-nm-sized nanogels coated with PAA/SPS films, obtaining an exponential variation of D and τ with the number of bilayers deposited.[27] Nevertheless, no trend was observed between the drug release mechanisms and D and τ values.

To understand the interplay of both variables in the drug release process, the dimensionless Deborah number, which relates the chain relaxation time (τ) to the diffusion time (θ), was determined according to the following equation

$$De = \frac{\tau}{\theta} \tag{1}$$

which may also be calculated by the ratio of the diffusion constant, k_F, and the relaxation constant, k_R (Table 1). The results from Table 2 indicate that De number trends well with the polymer relaxation contribution for some of the cases investigated, decreasing with the number of bilayers for the postassembly drug loading at pH 4.5 and increasing for the during-assembly method at pH 8.8. Peppas and Narasimhan highlighted that for systems in $De \ll 1$, the drug transport is considered Fickian or diffusion-controlled, while for $De \gg 1$, the drug transport is controlled by polymer chain relaxation.[37] This observation is in agreement with the data obtained in this study, which also shows an increase in the relaxation contribution for the drug release from PEM as De increases. However, it is still challenging to address the reason why the drug loading methods favor one mechanism of drug release transport over another.

The absorbance spectra after the drug release process may provide insights regarding the influence of the loading method into the drug interaction with the PEM matrix (Figure S4). In the release process, CAL molecules electrostatically interacting with amino groups of PAH chains are essentially washed out of the films due to the ionic exchange with anions in the PBS medium.[55] Absorbance spectra of the PEM at the end of the release experiment show the disappearance of the CAL peak at 505 nm, except for films assembled at pH 8.8 with post-assembled drug loading, possibly associated with a more stable

https://dx.doi.org/10.1021/acs.langmuir.0c01980
Langmuir 2020, 36, 12532−12544

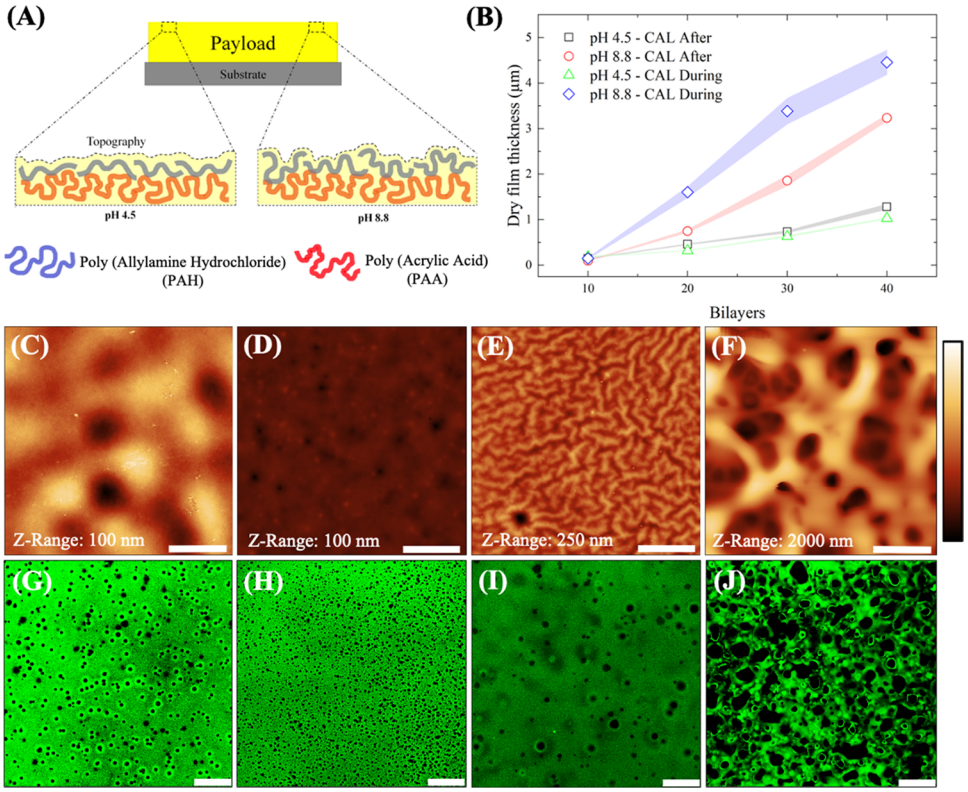

Figure 4. Interplay of the drug loading method and film morphology in PAA/PAH films. (A) Schematic representation of the complexation process that drives PEM assembly at pH 4.5 and pH 8.8. (B) Dry thickness results for PAA/PAH films assembled at different pH and drug loading methods. AFM images for PAA/PAH films assembled at pH 4.5 (C, D) and pH 8.8 (E, F) with postassembly and during-assembly drug loading methods, respectively. RMS surface roughness for AFM images are (C) (10.6 ± 2.1) nm, (D) (1.7 ± 0.2) nm, (E) (22.3 ± 4.3) nm, and (F) (427.5 ± 80.4) nm. Confocal microscopy images for PAA/PAH films assembled at pH 4.5 (G, H) and pH 8.8 (I, J) with postassembly and during-assembly drug loading methods, respectively. Bars in the AFM images correspond to 5 μm and in the confocal images correspond to 25 μm.

binding interaction between the CAL molecules and the PEM due to the multiple electrostatic binding sites of CAL molecules. Here, the more stable binding of CAL molecules and the PEM at pH 8.8 might be attributed to either the formation of several salt bridges of single polyprotic CAL molecules[50] with different PAH amino groups or the CAL adsorption into densely packed regions of the PEM.[56] As further discussed, changes in the CAL binding interaction with the PEM based on the film assembly condition method may cause significant impacts in the final drug release profile.

Influence of Drug Loading and Assembly Conditions in the Film Morphology. The effect of the chain conformation and ionization degree of weak polyelectrolytes may provide insights into the influence of the drug loading method on the release process. For weak polyelectrolytes, the solution ζ-potential and the particle size distribution are mediated by the solution pH, reflecting in the PEM morphology and, ultimately, in the drug loading and release properties.[34] Data on this subject are found in Figure S1.

Both polyelectrolytes present an increase in their particle size at their respective pK_a values (Figure S1B,C), which might be related to the loopy conformation of the uncharged polyelectrolyte segments as with the reduction in their ionization degree.[57] Solution ζ-potential measurements show a slight reduction in the ζ-potential at the respective pK_a value of each polyelectrolyte (Figure S1A), also reflecting a reduction in the amount of the ionized functional groups of the corresponding polyelectrolytes in the PEM structure. As opposed to the monomodal size distribution observed for PAA molecules, DLS results indicate that PAH molecules present two particle size populations at both assembly pH values tested (Figure S1B,C). The increase in the peak corresponding to the larger particles for PAH at pH 8.8 may explain the coarse-grained surface morphology of PAA/PAH films assembled at that condition (Figure S1E), contrasting with the flat surface observed for films assembled at pH 4.5 (Figure S1D). Figure 4A shows the schematic representation that summarizes the effect of the polyelectrolyte ionization degree on the polymer chain morphology and film topography.

The drug loading process also promoted a significant influence on both film thickness and surface morphology, particularly at pH 8.8, resulting in thicker films (Figure 4B) with irregular surface morphologies. This result may reflect the larger particle size for PAH at pH 8.8 observed in the DLS analysis. Shiratori and Rubner report the self-assembly of thicker films of PAA/PAH when one of the polyelectrolytes is fully ionized and the other one is partially ionized.[57] AFM images indicate that films assembled at pH 4.5 using both drug loading methods resulted in uniform surface morphology and lower surface roughness (Figure 4C,D). This morphology contrasts with the films assembled at pH 8.8, which presented a vermiculate-like surface (Figure 4E) for the postassembly drug loading method and a micrometer-pore-sized morphology for the drug loading during the film assembly (Figure 4F).

The substantial changes in film morphology observed at pH 8.8 with CAL loaded during the film assembly are possibly associated with the alternated switching in the pH environment from 8.8 to 7.1 during the PEM deposition and CAL loading

https://dx.doi.org/10.1021/acs.langmuir.0c01980
Langmuir 2020, 36, 12532−12544

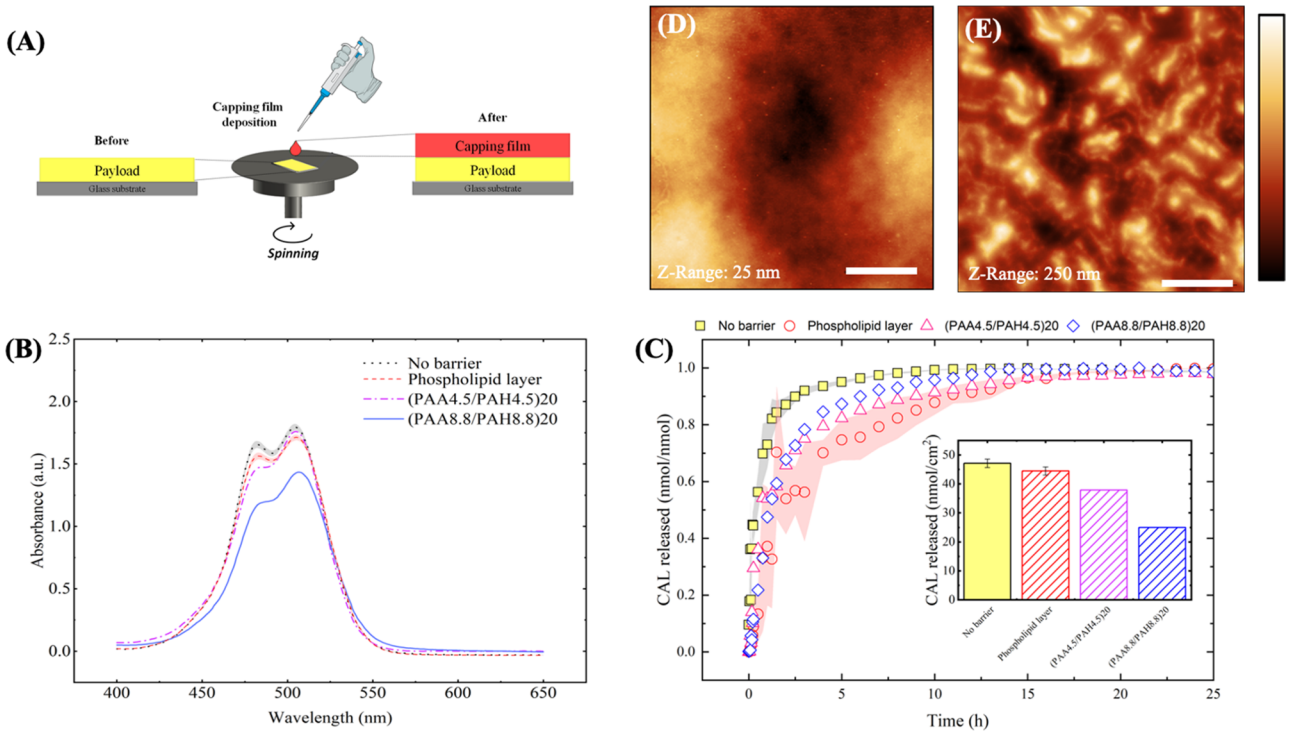

Figure 5. Deposition of the phospholipid capping layer reduces the drug release rate in PAA/PAH. (A) Schematic representation of the spin-coating deposition of a PEM or phospholipid capping film over the payload. (B) Absorbance spectra for the payload with and without the deposition of the capping films. (C) Drug release profiles for $(PAA4.5/PAH4.5)_{40}$ loaded with CAL after film assembly with and without capping film deposition. Shaded areas and error bars represent the standard error values. AFM images for (D) the payload only and the payload capped with a (E) phospholipid layer. Bars in the AFM images correspond to 5 μm. The corresponding surface RMS roughness values from AFM images are (D) (4.8 ± 1.6) nm and (E) (38.1 ± 0.9) nm.

process, respectively. Mendelsohn and co-workers described that the exposure of PAA/PAH films from a solution pH that differs from the assembly conditions modifies the ionization degree of the carboxylate groups from PAA.[36] This new configuration gives additional mobility to the PAA chains in the film bulk, enabling the rearrangement of the chains in an energetically and more favorable conformation, leaving fewer free ionized groups and a higher number of hydrophobic regions of the chains to interact with the solvent. The low affinity of the solvent with the hydrophobic regions of the electrostatic complex formed results in phase separation via spinodal decomposition, resulting in the structure with interconnected pores, characteristic of this separation phenomenon. The effect of the neutral solution on both chain mobility and film morphology is also reported in a previous paper.[41]

Confocal images (Figure 4G–J) for all assembly conditions tested indicate a homogeneous distribution of CAL over the entire film structure (see the confocal microscopy images for the axial region of the film in Figure S5), and some degree of micro-nanometer porosity in the film bulk, particularly for the during-assembly drug loading method. The assembly pH also seems to be relevant for the bulk morphology, promoting the formation of a nanoporous structure at pH 4.5 and a microporous structure at pH 8.8, both for the during-assembly drug loading method. The absence of interconnected pores at pH 4.5 suggests that a different phenomenon governs the reduction in the pore size for CAL loaded during the film assembly. The postassembly drug loading method also promoted some degree of porosity in the PEM structure to a minor extent.

Film morphology helps to explain some of the trends observed for the drug release process. The densely packed structure for films prepared using the postassembly drug loading method favors the diffusion over the polymer relaxation contribution in the drug release process as the number of bilayers increases. The porous morphology of films prepared with the during-assembly drug loading method, on the other hand, might explain the increasing contribution of the relaxation mechanism for the drug release process, taking into consideration the facilitated polymer matrix swelling by solvent diffusion through micro-to-nano-porous matrices.

Application of Spin-Coated Capping Films to Control the Drug Release Profile. PEM structures have also been explored as a capping film to promote a sustained drug release by changing the number of bilayers deposited,[27,58,59] the drug loading method,[34] and the release conditions.[59] Zhong and co-workers described the effect of the environmental pH and ionic strength, as well as the number of capping layers deposited, into the release of methylene blue from polypeptide films.[59] Dai and co-workers reported the use of alginate/PAH capping layers over different drug crystals, showing a decrease in the release rate with the number of bilayers deposited.[58] Despite the several studies that explore this topic, to our knowledge, there is a lack of studies investigating the influence of the assembly conditions of the capping layers on the drug release profile.

PAA/PAH films were deposited over a payload region, $(PAA4.5/PAH4.5)_{40}$ loaded with CAL loaded after film assembly, using the spin-coating LbL method, aiming to minimize the contact of the payload with the solvent to reduce drug leaking (Figure 5A). For the same purpose, the deposition of a phospholipid bilayer was also tested according to the parameters described elsewhere.[43] The absorbance spectra of the payload show a significant reduction on the CAL peak after

https://dx.doi.org/10.1021/acs.langmuir.0c01980
Langmuir 2020, 36, 12532−12544

$(PAA8.8/PAH8.8)_{20}$ capping film deposition, suggesting that an LbL-based strategy for capping film deposition promotes a significant reduction in the drug cargo, particularly at pH 8.8, where the PAA tends to displace a higher amount of drug from the payload (Figure 5B).

Release profiles showed a modest reduction in the drug release rate for the deposition of PAA/PAH films at pH 4.5 or 8.8 as capping layers and a more substantial decrease in the release rate observed for the deposition of the phospholipid layer over the payload (Figure 5C). Compared to the payload without the capping film, two of the cases investigated showed a significant loss in the amount of drug released (see the insets in Figure 5C). This result reflects the amount of drug lost during the deposition of the capping film, highlighting the importance of exploring film deposition strategies that reduce the number of steps and payload exposure to the solvent (see Figure S6 for CAL signal in PEM before the capping film deposition and after drug release).

The analysis of the fitted parameters for the three drug release models studied reinforces the qualitative analysis of the drug release profiles for the capped payload (Table 3). Both Higuchi and Ritger−Peppas models presented the more significant reduction in the release kinetic constant for the phospholipid capped films. The power-law model also presented an increase in the release exponent with the capping film deposition, changing the release mechanism from diffusion-controlled to anomalous after the barrier deposition, except for the phospholipid film. Finally, the Berens−Hopfenberg model indicated a reduction in the diffusional contribution for the drug release after the barrier deposition. Here, the relaxation contribution increases for all conditions tested, followed by an increase in the *De* number for the phospholipid- and the $(PAA4.5/PAH4.5)_{20}$-capped films.

To understand the influence of the PEM capping layers into the release kinetic constants, one may consider both their thickness and their chemical environment in the film bulk. Because films assembled at pH 8.8 are thicker than those assembled at pH 4.5 (see Figure 4B), one may expect a lower drug diffusion coefficient and, therefore, a lower release kinetic constant in films assembled at higher pH conditions. Tan and co-workers also reported smaller drug diffusion coefficient values for thicker PEM,[27] which corroborates with the data found here. Of note, the higher amount of free amino groups for films assembled at pH 8.8 than 4.5[57] may interact strongly with the negatively charged CAL molecules at pH 7.4, also hindering the drug release process. Similar factors may explain the phospholipid capping film results, which may have self-assembled into a membrane-like structure[43] with a polar head at the payload interface, covered by a densely packed hydrophobic layer of the nonpolar tails (see the larger packed structures distributed over the payload surface in the AFM images in Figure 5E). This membrane structure may also impair the drug release due to both the interactions of the carboxylate groups of CAL to the ionized amino groups of the phospholipid and the limited diffusivity of polar molecules of CAL throughout the densely packed nonpolar phospholipid membrane. These results highlight new possibilities to control the drug release profile by changing the thickness of the barrier and exploring the composition and assembly conditions of the building blocks forming the nanoarchitecture of the capping films.

CONCLUSION

This study shows the influence of the film assembly conditions and the drug loading method on the morphology and drug

Table 3. Influence of the Capping Film Deposition in the Release Model Parameters for $(PAA4.5/PAH4.5)_{40}$ Films Loaded with CAL After Film Assembly[a]

barrier assembly conditions	Higuchi		Ritger−Peppas			Berens−Hopfenberg						
	k_H	R^2	k_P	n	R^2	θ_F	k_F	θ_R	k_R	$D/10^{-15}$ (cm^2/s)	$\tau/10^4$ (s)	De	R^2
no barrier	0.839 (0.050)	0.858	0.786 (0.083)	0.436 (0.080)	0.851	0.774 (0.131)	0.649 (0.120)	0.225 (0.131)	4.200 (1.178)	75.22 (8.61)	0.085 (0.013)	0.154 (0.03)	0.982
phospholipid layer	0.258 (0.024)	0.738	0.340 (0.037)	0.369 (0.049)	0.816	0.279 (0.427)	0.795 (2.357)	0.720 (0.427)	0.204 (0.072)	92.15 (157.74)	1.758 (0.359)	3.886 (6.697)	0.970
$(PAA4.5/PAH4.5)_{20}$	0.483 (0.028)	0.902	0.481 (0.027)	0.598 (0.083)	0.909	0.637 (0.301)	0.653 (0.605)	0.362 (0.301)	0.163 (0.083)	75.64 (40.58)	2.204 (0.650)	3.998 (2.442)	0.976
$(PAA8.8/PAH8.8)_{20}$	0.425 (0.030)	0.880	0.412 (0.014)	0.839 (0.060)	0.978	0.123 (0.049)	0.081 (0.034)	0.876 (0.049)	0.602 (0.022)	9.497 (2.369)	0.597 (0.012)	0.136 (0.033)	0.996

[a]Standard error values are represented in parenthesis.

https://dx.doi.org/10.1021/acs.langmuir.0c01980
Langmuir 2020, 36, 12532−12544

release profile of PAA/PAH multilayers loaded with CAL via electrostatic interactions. Higher loading capacities were observed for the postassembly drug loading method at pH 8.8 due to the higher amount of freely ionized amino groups from PAH for electrostatic interaction with CAL. Higuchi and Ritger−Peppas models showed an increase in the release constant with the number of bilayers for the postassembly method at pH 8.8. The opposite trend was observed for the during-assembly drug loading method, attributed to the stronger binding of CAL molecules to the PEM due to the removal of moderate to weakly bound CAL molecules during the sequential assembly steps. The Berens−Hopfenberg model enabled us to decouple the contribution of different drug release mechanisms, indicating an increase in the diffusion contribution with the number of bilayers for the postassembly loading method at pH 4.5. The during-assembly drug loading method showed an increase of the relaxation contribution with the number of bilayers deposited at pH 8.8, possibly associated with the microstructured porous film structure that facilitates the swelling and polymer relaxation. For both cases, the dimensionless Deborah number follows the trends observed for the relaxation contribution. Furthermore, using a spin-coating method for the deposition of a capping film over the payload reduced both the initial burst release effect and drug release rate, favoring the polymer relaxation contribution mechanism, with the most substantial reduction for the densely packed phospholipid capping layer. In summary, this study sheds light on new alternatives to manipulate the drug release process of small molecules from thin films, highlighting new strategies to investigate the drug release mechanism in LbL films. These findings may support the design of materials with superior performance for drug delivery applications.

■ ASSOCIATED CONTENT

Supporting Information

The Supporting Information is available free of charge at https://pubs.acs.org/doi/10.1021/acs.langmuir.0c01980.

Polyelectrolyte solution properties (ζ-potential and particle size distribution from DLS measurements) and film morphology before drug loading (AFM images) (Figure S1); AFM-IR spectra for PAA/PAH films before and after CAL loading (Figure S2); the calibration curve for the CAL in PBS, the drug loading kinetic curve for PAA/PAH films, and the CAL solution spectra at different pH values (Figure S3); absorbance spectra for PAA/PAH films after CAL release (Figure S4); confocal images of axial positions for PAA/PAH films loaded with CAL (Figure S5); the absorbance spectra for PAA/PAH films before and after capping film deposition, and after the CAL release (Figure S6) (PDF)

■ AUTHOR INFORMATION

Corresponding Author

Rogério A. Bataglioli − *School of Chemical Engineering, University of Campinas, 13083-852 Campinas, SP, Brazil;* orcid.org/0000-0003-4987-1168; Email: rogerbataglioli@gmail.com

Authors

João Batista M. Rocha Neto − *School of Chemical Engineering, University of Campinas, 13083-852 Campinas, SP, Brazil*

Bruno S. Leão − *School of Chemical Engineering, University of Campinas, 13083-852 Campinas, SP, Brazil*

Luiz Guilherme L. Germiniani − *School of Chemical Engineering, University of Campinas, 13083-852 Campinas, SP, Brazil*

Thiago B. Taketa − *School of Chemical Engineering, University of Campinas, 13083-852 Campinas, SP, Brazil;* orcid.org/0000-0003-4861-1006

Marisa M. Beppu − *School of Chemical Engineering, University of Campinas, 13083-852 Campinas, SP, Brazil*

Complete contact information is available at: https://pubs.acs.org/10.1021/acs.langmuir.0c01980

Notes

The authors declare no competing financial interest.

■ ACKNOWLEDGMENTS

The authors acknowledge Sao Paulo Research Foundation (Grant Nos. 2016/10193-9 and 2018/20560-4 FAPESP) and CNPq (National Council for Scientific and Technological Development, Grant 147536/2016-2) for financial support. The authors also thank the Brazilian Nanotechnology National Laboratory (LNNano, CNPEM) for providing access to the AFM facilities.

■ REFERENCES

(1) Hao, X.; Chen, S.; Qin, D.; Zhang, M.; Li, W.; Fan, J.; Wang, C.; Dong, M.; Zhang, J.; Cheng, F.; Guo, Z. Antifouling and Antibacterial Behaviors of Capsaicin-Based PH Responsive Smart Coatings in Marine Environments. *Mater. Sci. Eng., C* **2020**, *108*, No. 110361.

(2) Iqbal, M. H.; Schroder, A.; Kerdjoudj, H.; Njel, C.; Senger, B.; Ball, V.; Meyer, F.; Boulmedais, F. Effect of the Buffer on the Buildup and Stability of Tannic Acid/Collagen Multilayer Films Applied as Antibacterial Coatings. *ACS Appl. Mater. Interfaces* **2020**, *12*, 22601−22612.

(3) Mak, W. C.; Cheung, K. Y.; Orban, J.; Lee, C. J.; Turner, A. P. F.; Griffith, M. Surface-Engineered Contact Lens as an Advanced Theranostic Platform for Modulation and Detection of Viral Infection. *ACS Appl. Mater. Interfaces* **2015**, *7*, 25487−25494.

(4) Soares, J. C.; Soares, A. C.; Rodrigues, V. C.; Melendez, M. E.; Santos, A. C.; Faria, E. F.; Reis, R. M.; Carvalho, A. L.; Oliveira, O. N. Detection of the Prostate Cancer Biomarker PCA3 with Electrochemical and Impedance-Based Biosensors. *ACS Appl. Mater. Interfaces* **2019**, *11*, 46645−46650.

(5) Rocha Neto, J. B. M.; Gomes Neto, R. J.; Bataglioli, R. A.; Taketa, T. B.; Pimentel, S. B.; Baratti, M. O.; Costa, C. A. R.; Carvalho, H. F.; Beppu, M. M. Engineering the Surface of Prostate Tumor Cells and Hyaluronan/Chitosan Multilayer Films to Modulate Cell-Substrate Adhesion Properties. *Int. J. Biol. Macromol.* **2020**, *158*, 197−207.

(6) Ghiorghita, C. A.; Bucatariu, F.; Dragan, E. S. Influence of Cross-Linking in Loading/Release Applications of Polyelectrolyte Multilayer Assemblies. A Review. *Mater. Sci. Eng., C* **2019**, *105*, No. 110050.

(7) Ariga, K.; Hill, J. P.; Ji, Q. Layer-by-Layer Assembly as a Versatile Bottom-up Nanofabrication Technique for Exploratory Research and Realistic Application. *Phys. Chem. Chem. Phys.* **2007**, *9*, 2319.

(8) Ariga, K.; Yamauchi, Y.; Rydzek, G.; Ji, Q.; Yonamine, Y.; Wu, K. C.-W.; Hill, J. P. Layer-by-Layer Nanoarchitectonics: Invention, Innovation, and Evolution. *Chem. Lett.* **2014**, *43*, 36−68.

(9) Zhong, Y.; Zeberl, B. J.; Wang, X.; Luo, J. Combinatorial Approaches in Post-Polymerization Modification for Rational Development of Therapeutic Delivery Systems. *Acta Biomater.* **2018**, *73*, 21−37.

(10) Wang, H.; Jia, L.; Cong, L.; Yu, H.; Wang, X. Enzymatically Mediated, Physiologically Triggered N-Palmitoyl Chitosan Hydrogels with Temporally Modulated High Injectability. *Colloids Surf., A* **2019**, *582*, No. 123940.

(11) Acharya, S.; Hill, J. P.; Ariga, K. Soft Langmuir-Blodgett Technique for Hard Nanomaterials. *Adv. Mater.* **2009**, *21*, 2959−2981.
(12) Casalini, S.; Bortolotti, C. A.; Leonardi, F.; Biscarini, F. Self-Assembled Monolayers in Organic Electronics. *Chem. Soc. Rev.* **2017**, *46*, 40−71.
(13) Decher, G. Fuzzy Nanoassemblies: Toward Layered Polymeric Multicomposites. *Science* **1997**, *277*, 1232−1237.
(14) Taketa, T. B.; Rocha Neto, J. B. M.; dos Santos, D. M.; Fiamingo, A.; Beppu, M. M.; Campana-Filho, S. P.; Cohen, R. E.; Rubner, M. F. Tracking Sulfonated Polystyrene Diffusion in a Chitosan/Carboxymethyl Cellulose Layer-by-Layer Film: Exploring the Internal Architecture of Nanocoatings. *Langmuir* **2020**, *36*, 4985−4994.
(15) Lee, H.; Gilbert, J. B.; Angilè, F. E.; Yang, R.; Lee, D.; Rubner, M. F.; Cohen, R. E. Design and Fabrication of Zwitter-Wettable Nanostructured Films. *ACS Appl. Mater. Interfaces* **2015**, *7*, 1004−1011.
(16) Jin, Y.; Zhou, Q.; Li, Z.; Yang, Z.; Fan, H.-J. S. Calcium-Cross Linked Polysaccharide Microcapsules for Controlled Release and Antimicrobial Applications. *Colloids Surf., A* **2020**, *600*, No. 125025.
(17) Macdonald, M.; Rodriguez, N. M.; Smith, R.; Hammond, P. T. Release of a Model Protein from Biodegradable Self Assembled Films for Surface Delivery Applications. *J. Controlled Release* **2008**, *131*, 228−234.
(18) Shi, H.; Zhang, R.; Feng, S.; Wang, J. Influence of Laponite on the Drug Loading and Release Performance of LbL Polyurethane/Poly(Acrylic Acid) Multilayers. *J. Appl. Polym. Sci.* **2019**, *136*, No. 47348.
(19) Yan, S.; Rao, S.; Zhu, J.; Wang, Z.; Zhang, Y.; Duan, Y.; Chen, X.; Yin, J. Nanoporous Multilayer Poly(l-Glutamic Acid)/Chitosan Microcapsules for Drug Delivery. *Int. J. Pharm.* **2012**, *427*, 443−451.
(20) Anirudhan, T. S.; Vasantha, C. S.; Sasidharan, A. Layer-by-Layer Assembly of Hyaluronic Acid/Carboxymethylchitosan Polyelectrolytes on the Surface of Aminated Mesoporous Silica for the Oral Delivery of 5-Fluorouracil. *Eur. Polym. J.* **2017**, *93*, 572−589.
(21) Wang, S.; Battigelli, A.; Alkekhia, D.; Fairman, A.; Antoci, V.; Yang, W.; Moore, D.; Shukla, A. Controlled Delivery of a Protein Tyrosine Phosphatase Inhibitor, SHP099, Using Cyclodextrin-Mediated Host-Guest Interactions in Polyelectrolyte Multilayer Films for Cancer Therapy. *RSC Adv.* **2020**, *10*, 20073−20082.
(22) Zhang, S.; Xing, M.; Li, B. Capsule-Integrated Polypeptide Multilayer Films for Effective pH-Responsive Multiple Drug Co-Delivery. *ACS Appl. Mater. Interfaces* **2018**, *10*, 44267−44278.
(23) Uppu, D. S. S. M.; Turvey, M. E.; Sharif, A. R. M.; Bidet, K.; He, Y.; Ho, V.; Tambe, A. D.; Lescar, J.; Tan, E. Y.; Fink, K.; Chen, J.; Hammond, P. T. Temporal Release of a Three-Component Protein Subunit Vaccine from Polymer Multilayers. *J. Controlled Release* **2020**, *317*, 130−141.
(24) San Juan, A. M. T.; Rodgers, T.; Bedolla, C.; Noriega, F.; Romero, G. Layer by Layer Surface Engineering of Poly(Lactide-Co-Glycolide) Nanoparticles for Plasmid DNA Delivery. *J. Appl. Polym. Sci.* **2020**, *137*, No. 49377.
(25) Mirgorodskaya, A. B.; Kushnazarova, R. A.; Nikitina, Av.; Semina, I. I.; Nizameev, I. R.; Kadirov, M. K.; Khutoryanskiy, V. V.; Zakharova, L. Y.; Sinyashin, O. G. Polyelectrolyte Nanocontainers: Controlled Binding and Release of Indomethacin. *J. Mol. Liq.* **2018**, *272*, 982−989.
(26) Kamburova, K.; Mitarova, K.; Radeva, T. Polysaccharide-Based Nanocapsules for Controlled Release of Indomethacin. *Colloids Surf., A* **2017**, *519*, 199−204.
(27) Tan, J. P. K.; Wang, Q.; Tam, K. C. Control of Burst Release from Nanogels via Layer by Layer Assembly. *J. Controlled Release* **2008**, *128*, 248−254.
(28) Gonzalez, J. S.; Mijangos, C.; Hernandez, R. Polysaccharide Coating of Gelatin Gels for Controlled BSA Release. *Polymers* **2019**, *11*, No. 702.
(29) Cuomo, F.; Ceglie, A.; Piludu, M.; Miguel, M. G.; Lindman, B.; Lopez, F. Loading and Protection of Hydrophilic Molecules into Liposome-Templated Polyelectrolyte Nanocapsules. *Langmuir* **2014**, *30*, 7993−7999.
(30) Jeon, S.; Yoo, C. Y.; Park, S. N. Improved Stability and Skin Permeability of Sodium Hyaluronate-Chitosan Multilayered Liposomes by Layer-by-Layer Electrostatic Deposition for Quercetin Delivery. *Colloids Surf., B* **2015**, *129*, 7−14.
(31) Li, H.; Zhu, X.; Xu, J.; Peng, W.; Zhong, S.; Wang, Y. The Combination of Adsorption by Functionalized Halloysite Nanotubes and Encapsulation by Polyelectrolyte Coatings for Sustained Drug Delivery. *RSC Adv.* **2016**, *6*, 54463−54470.
(32) Chen, P.; Song, H.; Yao, S.; Tu, X.; Su, M.; Zhou, L. Magnetic Targeted Nanoparticles Based on β-Cyclodextrin and Chitosan for Hydrophobic Drug Delivery and a Study of Their Mechanism. *RSC Adv.* **2017**, *7*, 29025−29034.
(33) Wood, K. C.; Boedicker, J. Q.; Lynn, D. M.; Hammond, P. T. Tunable Drug Release from Hydrolytically Degradable Layer-by-Layer Thin Films. *Langmuir* **2005**, *21*, 1603−1609.
(34) Chung, A. J.; Rubner, M. F. Methods of Loading and Releasing Low Molecular Weight Cationic Molecules in Weak Polyelectrolyte Multilayer Films. *Langmuir* **2002**, *18*, 1176−1183.
(35) Berg, M. C.; Zhai, L.; Cohen, R. E.; Rubner, M. F. Controlled Drug Release from Porous Polyelectrolyte Multilayers. *Biomacromolecules* **2006**, *7*, 357−364.
(36) Mendelsohn, J. D.; Barrett, C. J.; Chan, V. V.; Pal, A. J.; Mayes, A. M.; Rubner, M. F. Fabrication of Microporous Thin Films from Polyelectrolyte Multilayers. *Langmuir* **2000**, *16*, 5017−5023.
(37) Peppas, N. A.; Narasimhan, B. Mathematical Models in Drug Delivery: How Modeling Has Shaped the Way We Design New Drug Delivery Systems. *J. Controlled Release* **2014**, *190*, 75−81.
(38) Higuchi, T. Rate of Release of Medicaments from Ointment Bases Containing Drugs in Suspension. *J. Pharm. Sci.* **1961**, *50*, 874−875.
(39) Ritger, P. L.; Peppas, N. A. A Simple Equation for Description of Solute Release I. Fickian and Non-Fickian Release from Non-Swellable Devices in the Form of Slabs, Spheres, Cylinders or Discs. *J. Controlled Release* **1987**, *5*, 23−36.
(40) Berens, A. R.; Hopfenberg, H. B. Diffusion and Relaxation in Glassy Polymer Powders: 2. Separation of Diffusion and Relaxation Parameters. *Polymer* **1978**, *19*, 489−496.
(41) Bataglioli, R. A.; Taketa, T. B.; Neto, J. B. M. R.; Lopes, L. M.; Costa, C. A. R.; Beppu, M. M. Analysis of PH and Salt Concentration on Structural and Model-Drug Delivery Properties of Polysaccharide-Based Multilayered Films. *Thin Solid Films* **2019**, *685*, 312−320.
(42) Martins, T. D.; Bataglioli, R. A.; Taketa, T. B.; da Cruz Vasconcellos, F.; Beppu, M. M. Surface Modification of Polyelectrolyte Multilayers by High Radio Frequency Air Plasma Treatment. *Appl. Surf. Sci.* **2015**, *329*, 287−291.
(43) Mennicke, U.; Salditt, T. Preparation of Solid-Supported Lipid Bilayers by Spin-Coating. *Langmuir* **2002**, *18*, 8172−8177.
(44) Yoo, D.; Shiratori, S. S.; Rubner, M. F. Controlling Bilayer Composition and Surface Wettability of Sequentially Adsorbed Multilayers of Weak Polyelectrolytes. *Macromolecules* **1998**, *31*, 4309−4318.
(45) Lichter, J. A.; Rubner, M. F. Polyelectrolyte Multilayers with Intrinsic Antimicrobial Functionality: The Importance of Mobile Polycations. *Langmuir* **2009**, *25*, 7686−7694.
(46) Hiller, J.; Mendelsohn, J. D.; Rubner, M. F. Reversibly Erasable Nanoporous Anti-Reflection Coatings from Polyelectrolyte Multilayers. *Nat. Mater.* **2002**, *1*, 59−63.
(47) Quinn, J. F.; Yeo, J. C. C.; Caruso, F. Layer-by-Layer Assembly of Nanoblended Thin Films: Poly(Allylamine Hydrochloride) and a Binary Mixture of a Synthetic and Natural Polyelectrolyte. *Macromolecules* **2004**, *37*, 6537−6543.
(48) Petrov, A. I.; Antipov, A. A.; Sukhorukov, G. B. Base-Acid Equilibria in Polyelectrolyte Systems: From Weak Polyelectrolytes to Interpolyelectrolyte Complexes and Multilayered Polyelectrolyte Shells. *Macromolecules* **2003**, *36*, 10079−10086.
(49) Tokudome, Y.; Sugibayashi, K. Mechanism of the Synergic Effects of Calcium Chloride and Electroporation on the in Vitro Enhanced Skin Permeation of Drugs. *J. Controlled Release* **2004**, *95*, 267−274.

https://dx.doi.org/10.1021/acs.langmuir.0c01980
Langmuir 2020, 36, 12532−12544

(50) Furry, J. Preparation, Properties and Applications of Calcein in a Highly Pure Form. Thesis; 1985.
(51) Wallach, D. F. H.; Surgenor, D. M.; Soderberg, J.; Delano, E. Preparation and Properties of 3, 6-Dihydroxy-2,4-Bis-[N,N′-Di-(Carboxymethyl)-Aminomethyl] Fluoran. *Anal. Chem.* **1959**, *31*, 456−460.
(52) Ladam, G.; Schaad, P.; Voegel, J. C.; Schaaf, P.; Decher, G.; Cuisinier, F. In Situ Determination of the Structural Properties of Initially Deposited Polyelectrolyte Multilayers. *Langmuir* **2000**, *16*, 1249−1255.
(53) Wang, F.; Li, J.; Tang, X.; Huang, K.; Chen, L. Polyelectrolyte Three Layer Nanoparticles of Chitosan/Dextran Sulfate/Chitosan for Dual Drug Delivery. *Colloids Surf., B* **2020**, *190*, No. 110925.
(54) Zhao, Q.; Han, B.; Wang, Z.; Gao, C.; Peng, C.; Shen, J. Hollow Chitosan-Alginate Multilayer Microcapsules as Drug Delivery Vehicle: Doxorubicin Loading and in Vitro and in Vivo Studies. *Nanomed.: Nanotechnol. Biol. Med.* **2007**, *3*, 63−74.
(55) Haidar, Z. S.; Hamdy, R. C.; Tabrizian, M. Protein Release Kinetics for Core-Shell Hybrid Nanoparticles Based on the Layer-by-Layer Assembly of Alginate and Chitosan on Liposomes. *Biomaterials* **2008**, *29*, 1207−1215.
(56) Costa, R. R.; Custódio, C. A.; Arias, F. J.; Rodríguez-Cabello, J. C.; Mano, J. F. Nanostructured and Thermoresponsive Recombinant Biopolymer-Based Microcapsules for the Delivery of Active Molecules. *Nanomed.: Nanotechnol. Biol. Med.* **2013**, *9*, 895−902.
(57) Shiratori, S. S.; Rubner, M. F. PH-Dependent Thickness Behavior of Sequentially Adsorbed Layers of Weak Polyelectrolytes. *Macromolecules* **2000**, *33*, 4213−4219.
(58) Dai, Z.; Heilig, A.; Zastrow, H.; Donath, E.; Möhwald, H. Novel Formulations of Vitamins and Insulin by Nanoengineering of Polyelectrolyte Multilayers around Microcrystals. *Chem. − Eur. J.* **2004**, *10*, 6369−6374.
(59) Zhong, Y.; Whittington, C. F.; Zhang, L.; Haynie, D. T. Controlled Loading and Release of a Model Drug from Polypeptide Multilayer Nanofilms. *Nanomed.: Nanotechnol. Biol. Med.* **2007**, *3*, 154−160.

https://dx.doi.org/10.1021/acs.langmuir.0c01980
Langmuir 2020, 36, 12532−12544